Integrated Polarization Analyzing CMOS Image Sensor for Material Classification

Mukul Sarkar, *Student Member, IEEE*, David San Segundo Bello, *Member, IEEE*, Chris van Hoof, *Member, IEEE*, and Albert Theuwissen, *Fellow, IEEE*

***Abstract*—Material classification is an important application in computer vision. The inherent property of materials to partially polarize the reflected light can serve as a tool to classify them. In this paper, a real-time polarization sensing CMOS image sensor using a wire grid polarizer is proposed. The image sensor consist of an array of 128 × 128 pixels, occupies an area of 5 × 4 mm^2 and it has been designed and fabricated in a 180-nm CMOS process. We show that this image sensor can be used to differentiate between metal and dielectric surfaces in real-time due to the different nature in partially polarizing the specular and diffuse reflection components of the reflected light. This is achieved by calculating the Fresnel reflection coefficients, the degree of polarization and the variations in the maximum and minimum transmitted intensities for varying specular angle of incidence. Differences in the physical parameters for various metal surfaces result in different surface reflection behavior, influencing the Fresnel reflection coefficients. It is also shown that the image sensor can differentiate among various metals by sensing the change in the polarization Fresnel ratio.**

***Index Terms*—degree of polarization, Fresnel reflection coefficients, image sensor, material classification, polarization, stokes parameters, wire grid polarizer.**

I. Introduction

A. Material Classification

INFORMATION on the type of material can provide important information about the scene in computer or machine vision applications. Materials can be broadly classified into metals and dielectrics, based on their conductivity. Metals are highly conductive, opaque, and tend to be very reflective while dielectrics are less conductive and have very low reflectivity.

Earlier attempts to distinguish between metals and dielectrics used the dichromatic reflection properties of the material surface [1]–[3]. Materials were classified into optically homogenous or optically inhomogeneous. Healey [4] showed that homogenous materials reflect light only from the surface. Thus, when such materials are illuminated with a monochromatic light beam they reflect light of a fixed color (wavelength). Inhomogeneous materials on the other hand reflect light from the surface and also scatter light from the body. Such a material, when illuminated with a monochromatic light beam would reflect two distinct colors, one being the reflected color from the surface while the other being the color of the light scattered from the body. Based on the number of reflected colors the objects can be classified as homogenous or inhomogeneous. Once the object has been determined to be either homogenous or inhomogeneous, it can be further classified as a metal or a dielectric depending on the reflected color. Metals have free electrons, and when these electrons are hit by a light ray the resulting response of the electrons is a function of the wavelength of the light ray. Some metals such as steel and nickel produce near uniform response for changes in the wavelength over the entire visible spectrum while certain metals such as copper and gold tend to reflect longer wavelengths more than the shorter ones. Dielectrics on the other hand do not have free electrons thus the reflectivity from a dielectric surface is independent of the wavelength of the incident light ray. This method, however, is limited by the distortion of the color histogram obtained after reflection, which depends on the object geometry. Additionally, the color of the material also influences the reflected color.

Another method to discriminate between metals and dielectrics is based on the Fresnel reflection theory which was proposed by Wolff [5], [6]. According to this theory, dielectric surfaces polarize the light upon specular reflection stronger than metal surfaces for all angles of incidence. The Fresnel reflection coefficients are used to compute the polarization Fresnel ratio (PFR), which is shown to be equal to the ratio of the maximum to the minimum transmitted irradiance at the material surface [5]. The PFR is used to classify materials into metals and dielectrics. The maximum and minimum transmitted irradiances are obtained by allowing the reflected light from the material surface to pass through an external linear polarizer onto a CCD or CMOS image sensor. The disadvantage of such a system is that the linear polarization filters have to be externally controlled, which complicates the automation and miniaturization of optical sensors for material classification. Additionally, the PFR is computed using digital processing blocks which increase the overall power consumption of the system.

B. Polarization Image Sensors

State-of-the-art of polarization image sensors consists of either a standard CMOS/CCD camera coupled with an external

Manuscript received June 11, 2010; revised October 13, 2010; accepted November 13, 2010. Date of publication November 29, 2010; date of current version May 25, 2011. The associate editor coordinating the review of this paper and approving it for publication was Prof Kiseon Kim.

M. Sarkar is with imec, 5656 AE, Eindhoven, The Netherlands, and also with the Electronic Instrumentation Laboratory, Delft University of Technology, 2628 CD Delft, The Netherlands (e-mail: mukul.sarkar@imec-nl.nl).

D. San Segundo and C. Van Hoof are with imec, 3001 Leuven, Belgium (e-mail: david.sansegundobello@imec.be; chris.vanhoof@imec.be).

A. J. P. Theuwissen is with Harvest Imaging, 3960 Bree, Belgium, and also with the Electronic Instrumentation Laboratory, Delft University of Technology, 2628 CD Delft, The Netherlands (e-mail: a.j.p.theuwissen@tudelft.nl).

Color versions of one or more of the figures in this paper are available online at http://ieeexplore.ieee.org.

Digital Object Identifier 10.1109/JSEN.2010.2095003

polarization filter, or on integrated polarization filters fabricated on top of the pixel array. The latter can measure polarization information in real time.

From the aperture theory [7], [8], it is known that for an electromagnetic wave to be absorbed by a wire grid, its wavelength should be larger than the pitch of the wire grid ($\lambda/d > 2$; where λ is the wavelength and d is the spacing between the wire grid). To obtain the polarization information in the visible spectrum, a wire grid pitch of less than 300 nm is desired. With the scaling of CMOS technologies, the minimum distance between metal wires also scales, opening up the possibility of using them in a grid structure for the absorption of electromagnetic waves, thus polarizing the transmitted wave. An embedded wire grid polarizer with an extinction ratio of 2.03 has already been demonstrated [9], [10]. The wire grid pitch used was 1.2 μm. An integrated polymer polarization filter array with a pitch of 6 μm has also been reported [11].

In this paper, we present a CMOS image sensor with real time polarization sensing ability using a metal wire grid of pitch 0.48 μm. The image sensor uses the model proposed in [5] and [6] to classify materials based on the polarization information.

The theory behind Fresnel coefficients is covered in Section II. In Section III, the CMOS image sensor is described. Section IV presents the measured transmittance of the wire grid polarizer. Section V describes the methods for material classification. Section VI concludes the paper and outlines the future work.

II. Theory

A. Polarization and Fresnel Coefficients

Electromagnetic radiation travels as transverse waves, i.e., waves that vibrate in a direction perpendicular to their direction of propagation. Polarization is a phenomenon peculiar to transverse waves based on the distribution of the electric field in the plane normal to the propagation direction. In an unpolarized or randomly polarized electromagnetic wave the orientation of the electric vector changes randomly.

A mathematical representation of a plane wave propagating in the z direction is given as

$$E = E_0 \cos(kz - \omega t + \varphi_0) \tag{1}$$

where E_0 is the amplitude, k is the propagation (or wave) constant ($k = 2\pi/\lambda$), ω is the circular frequency ($\omega = kc = 2\pi c/\lambda$), and φ_0 is the initial phase.

An unpolarized electromagnetic wave can be polarized through absorption, reflection, refraction, and scattering. In this paper, we will focus our discussion to polarization of electromagnetic waves by reflection. The polarization by reflection from a material surface depends on the angle at which the light strikes the reflecting surface as well as on the nature of said surface. Metallic surfaces reflect light with a variety of vibration directions, and such reflected light is usually unpolarized. However, nonmetallic surfaces reflect light such that the vibrations of the reflecting light wave is parallel to the plane of the reflecting surface.

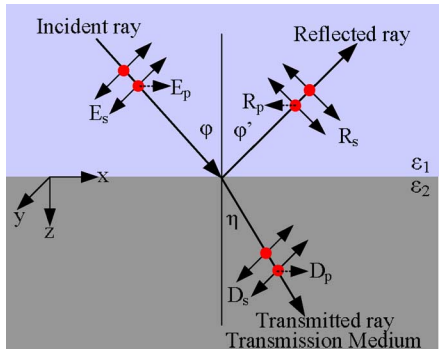

Fig. 1. Incident, reflected, and transmitted Fresnel coefficients.

Polarization can either be elliptical, circular or linear in nature. Elliptical polarized light consists of two perpendicular waves of unequal amplitude which differ in phase by 90°. If the perpendicular waves are of equal amplitude it results in a circularly polarized light. A linearly polarized wave has its electric field vibrating in the same direction at all times at a particular point. Elliptical and circular polarizations are more uncommon in nature than linear polarization. Furthermore, since a wire grid allows only a specific polarization to pass through, the transmitted wave will have a single linear polarization and thus only the linear polarization in considered in this work.

When a light ray strikes a surface, part of the incident light is reflected and part is transmitted or absorbed as shown in Fig. 1, φ is the angle of incidence of the incident ray, φ' is the angle of reflection of the reflected ray and η is the angle of transmission of the transmitted ray.

The reflection occurring at the surface of the planar surface can be divided into diffuse and specular. When light strikes a surface, part of the light passes through the boundary, which is re-emitted randomly. Diffuse reflection is caused by the reflected rays from internal scattering inside the surface medium. The diffuse reflection component is independent of the angle of reflection but depends on the angle of incidence.

Specular reflection is a mirror-like reflection from the surface, in which light from a single incoming direction is reflected into a single outgoing direction. Pure specular reflection occurs when the planar interface portion of the surface is significantly larger than the wavelength of the incident light [5]. The incident and the reflected directions of the specularly reflected light determine the specular plane of incidence.

Unpolarized light becomes partially polarized after specular reflection. The incident electric field can be split into two components, one perpendicular to the plane of incidence with amplitude E_s and the other parallel to the plane of incidence with amplitude E_p as shown in Fig. 1. When the incident transverse wave reaches the boundary between the mediums, it is divided into a reflected and a refracted wave component. The fraction of the incident light that is reflected from the interface is given by the reflection coefficients R, and the fraction that is refracted is given by the refraction coefficients D. Since the incident light has polarized components, the reflected and the refracted light will also have polarized components which are expressed in

terms of the Fresnel reflection coefficients. The Fresnel reflection equations are expressed as

$$\begin{aligned} R_s &= -E_s \frac{\sin(\varphi-\eta)}{\sin(\varphi+\eta)} \\ R_p &= -E_p \frac{\tan(\varphi-\eta)}{\tan(\varphi+\eta)} \\ D_s &= E_s \frac{2\sin\eta\cos\varphi}{\sin(\varphi+\eta)} \\ D_p &= E_p \frac{2\sin\eta\cos\varphi}{\sin(\varphi+\eta)\cos(\varphi-\eta)}. \end{aligned} \tag{2}$$

R_P, R_S, D_P and D_S are the reflection and refraction coefficients, $\varphi^{'}$ is the angle of reflection, and η is the angle of refraction.

The Fresnel coefficients are used to describe the amount of light reflected or transmitted from a surface and form the basis of Fresnel reflectance model discussed in Section II-B. The polarization of the light wave expressed by (1) and also the polarized reflected and transmitted components in (2) describe the polarization in terms of its amplitude. The amplitude of the optical field cannot be observed, but it is possible to observe and measure the intensity which is the time average of the square of the field amplitudes. The Stokes parameters which are used to represent the polarization in terms of the intensity of the light wave are discussed further in Section II-C.

B. Fresnel Reflectance Model

The reflectance model describes the intensity and spectral composition of the light reflected from the reflection surface and reaching the observer. The intensity of the reflected light depends on the intensity and size of the light source and also on the surface properties of the material. The spectral composition of the reflected light is determined by the wavelength selective reflection of the surface.

When the reflected wave component is passed through a linear polarizer, the intensity of the image can be expressed as a function of the transmission axis of the polarizer (θ) [5]. The spectral transmittances of the polarizer for linearly polarized light and unpolarized light are denoted by $T_p(\lambda)$ and $T_n(\lambda)$, respectively, where λ is the wavelength of the light.

The intensity image of the reflected light from the surface is expressed in terms of the pixel coordinates (x, y) and the transmission axis of the polarizer. The intensity image obtained after the reflection can be written as a sum of the diffuse reflection coefficient $I_d(x, y)$ and the specular reflection coefficient $I_s(x, y)$ [5], [13]. Using the Fresnel reflection (2), the intensity image observed through the polarizer transmission axis θ can be expressed as shown in (3) at the bottom of the page, where θ_0 is the direction perpendicular to the specular plane. The Fresnel reflection coefficients R_p and R_s depend on the pixel coordinates. In terms of polarized and unpolarized components, (3) can be rewritten as

$$I(x, y:\theta) = A(x, y)\frac{1+\cos 2(\theta-\theta_0)}{2} + B(x, y) \tag{4}$$

where

$$A(x, y) = \frac{R_p(x, y) - R_s(x, y)}{R_p(x, y) + R_s(x, y)} T_p I_s(x, y) \tag{5}$$

$$B(x, y) = \frac{R_p(x, y)}{R_p(x, y) + R_s(x, y)} T_p I_s(x, y) + T_n I_d(x, y) \tag{6}$$

It can be observed from (4) that $I(x, y : \theta)$ oscillates as θ varies between the maximum $I_{\max}(x, y)$ at $\theta = \theta_0, \theta_0 + \pi$ and the minimum $I_{\min}(x, y)$ at $\theta = \theta_0 \pm \pi/2$. $I_{\max}(x, y)$ and $I_{\min}(x, y)$ are then expressed in terms of (5) and (6) as

$$\begin{aligned} &I_{\max}(x, y) \\ &\quad = A(x, y) + B(x, y) \\ &\quad = \frac{R_s(x, y)}{R_p(x, y) + R_s(x, y)} T_p I_s(x, y) + T_n I_d(x, y) \end{aligned} \tag{7}$$

$$\begin{aligned} &I_{\min}(x, y) \\ &\quad = B(x, y) \\ &\quad = \frac{R_p(x, y)}{R_p(x, y) + R_s(x, y)} T_p I_s(x, y) + T_n I_d(x, y) \end{aligned} \tag{8}$$

The first term in (4) is the polarized component of the reflection mainly contributed by the specular reflection of the incident transverse wave. The second term represents the unpolarized component contributed by the diffuse reflections and partly by the specular reflection which is not polarized.

C. Stokes Parameters and Degree of Polarization

The polarization state of an electromagnetic wave can be conveniently described by the Stokes parameters. These parameters were developed in 1852 by G. G. Stokes and are widely used to represent the partial polarization states. The four Stokes parameters are grouped into the Stokes vector as shown as

$$\vec{S} = \begin{bmatrix} S_0 \\ S_1 \\ S_2 \\ S_3 \end{bmatrix} = \begin{bmatrix} I \\ Q \\ U \\ V \end{bmatrix}. \tag{9}$$

The Stokes parameters represented in (9) are intensity (I), degree of polarization (Q), plane of polarization (U), and ellipticity (V).

The vector components are given by

$$\begin{aligned} S_0 &= E_{x0}^2 + E_{y0}^2 \\ S_1 &= E_{x0}^2 - E_{y0}^2 \\ S_2 &= 2E_{x0}E_{y0}\cos(\nabla\varphi) \\ S_3 &= 2E_x E_y \sin(\nabla\varphi) \end{aligned} \tag{10}$$

$$I(x, y:\theta) = T_n I_d(x, y) + T_p \frac{R_p(x, y)\sin^2(\theta-\theta_0) + R_s(x, y)\cos^2(\theta-\theta_0)}{R_p(x, y) + R_s(x, y)} \times I_s(x, y) \tag{3}$$

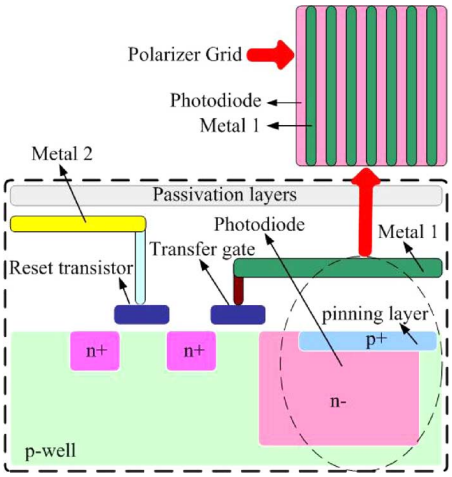

Fig. 2. Wire grid polarizer.

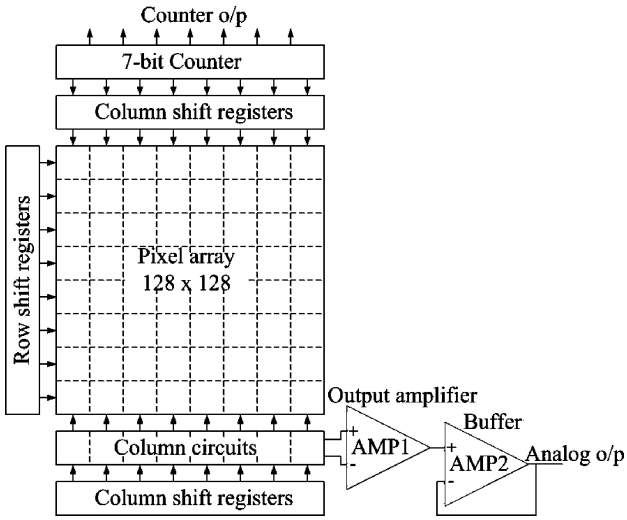

Fig. 3. Sensor architecture.

where E_{x0} is the field strength of parallel polarized light, E_{y0} is the field strength of perpendicular polarized light, and $\nabla\varphi$ is the phase difference between the parallel and perpendicular polarized light.

There are two ways to express the partial polarization: the degree of polarization (DOP) and the Jones coherency matrix J [12]. The degree of polarization is a measure of the percentage of the electric field of light which is polarized compared to the electric field of total incident light. DOP is a scalar value between 0 and 1, and will be used to express the partial polarization in this work [12], [14]. In terms of Stokes parameters, the degree of polarization (DOP) of the light beam is expressed as

$$\text{DOP} = \delta = \frac{\sqrt{S_1^2 + S_2^2 + S_3^2}}{S_0}. \tag{11}$$

Three states of polarization of a light wave are possible: completely unpolarized, completely polarized, or partially polarized. A completely polarized light in terms of Stokes parameters is represented by $S_0^2 = S_1^2 + S_2^2 + S_3^2$ and a DOP of 1. For a completely unpolarized light, the Stokes parameters satisfy $S_1 = S_2 = S_3 = 0$ and $\text{DOP} = 0$. A partially polarized light satisfies $S_0^2 > S_1^2 + S_2^2 + S_3^2$.

In a linearly polarized light beam, circular and elliptical polarizations do not usually occur, its degree of polarization is thus often referred to as degree of linear polarization. The degree of linear polarization (DOLP) of a light beam is defined by

$$\text{DOLP} = \frac{S_1}{S_0}. \tag{12}$$

III. Sensor Description

The image sensor consists of an array of 128 by 128 pixels, it occupies an area of 5×4 mm^2 and it has been designed and fabricated in the 180-nm CMOS CIS process from UMC. The sensor has an embedded linear wire grid polarizer in each pixel, realized with the first metal layer of the process on top of a pinned photodiode (p^+/n^-/p-sub). The linear wire grid polarizer was implemented using thin metal strips with a line/space of 240 nm/240 nm (pitch of 480 nm) as shown in Fig. 2. Although a pitch of less than 300 nm is required to cover the complete visible spectrum wavelength range, the chosen technology allows only for a pitch of 480 nm.

TABLE I
Sensor Specifications

Process	0.18μm 1 poly 3 metals UMC CIS process
On-chip Polarizer	Line/Space = 240nm/ 240nm (480nm pitch)
Active imager size	3.2 mm(H) x 3.2 mm(V)
Chip Size	4 mm(H) x 5 mm(V)
Active pixels	128 x 128
Pixel size	25μm x 25μm
Shutter type	Global shutter
Maximum data rate/master clock	64 MPS / 32 MHz
Supply voltage	1.8V

Fig. 3 shows the sensor architecture. Table I lists the sensor specifications.

The chip is divided into four main blocks: the pixel array, the analog readout, the digital readout and the row select logic and timing control. The pixel array with the photodiodes and the associated circuitry for analog computations occupies most of the chip area. Each pixel contains a pinned photodiode and 32 transistors to perform low level image processing. In this paper we focus on the polarization sensing ability of the designed image sensor and thus the low level image processing will not be discussed. The size of the photodiode is 10 μm $\times$ 10 μm which corresponds to a 16% pixel fill factor. Placed below the pixel array is the analog readout circuit, which consists of column level circuits (double differential sampling circuit), an output amplifier, a buffer and the column shift register. Placed at the top is the digital readout circuit, which consists of a 7-bit counter and a column shift register. The 7-bit counter is used to count the number of active high pixels in each row. Finally, the left side is dedicated to a row select logic and timing control blocks to address each row of pixels sequentially.

The array of 128 by 128 pixels was split into three regions as shown in Fig. 4.

1) A 64×128 array without a metal grid used for normal imaging applications.

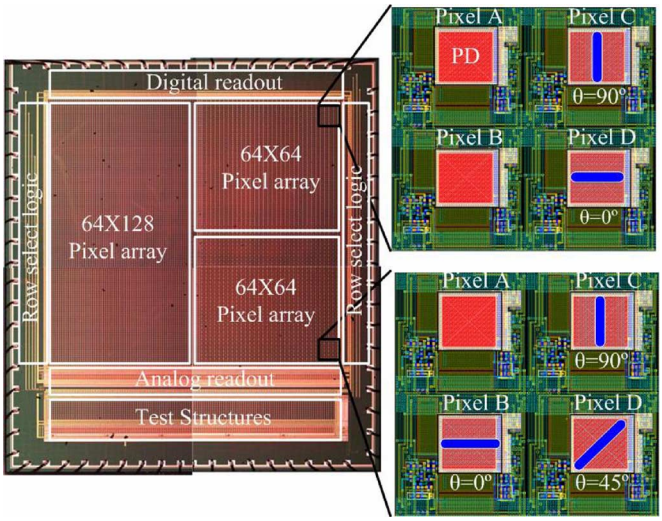

Fig. 4. Sensor regions with different polarizing angles.

2) A 64 × 64 array (sense region 1) consisting of 2 by 2 pixel arrays where two pixels (A and B) measure the intensity while the other two measure the 0°(D), and 90°(C) polarized intensity, respectively.
3) A 64 × 64 array (sense region 2) consisting of 2 by 2 pixel arrays where one pixel records the intensity of the light (A) while the other 3 record the 0°(B), 45°(C) and 90°(D) polarized intensity.

The additional pixel sensitivity to 45° polarized light in sense region 2 is used to compute the Stokes parameters. The pixels dedicated to sense the intensity in regions 1 and 2 are used to normalize the data obtained from the pixels sensitive to polarization directions.

IV. Transmittance Measurements

Linear polarizers are characterized by two main specifications: transmittance and contrast or extinction ratio. The transmittance is the percentage of light that passes through the linear polarizer. The contrast or extinction ratio is defined as the ratio of the power of a plane-polarized beam that is transmitted through a polarizer placed in its path with its polarizing axis parallel to the plane of the beam, as compared with the transmitted power when the polarizer axis is perpendicular to the plane of the beam.

In order to characterize the sensor, we used a polarized light obtained by passing the light from a dc light source through a linear polarizer. The transmission axis of the linear polarizer is varied from 0° to 180° in steps of 15° to change the polarization angle of the light reaching the image sensor. The corresponding analog output of the pixels sensitive to 0° and 90° in the polarization sense region 1 and 0°, 45°, and 90° in the polarization sense region 2 are stored. The obtained analog output is normalized with respect to the intensity obtained at the intensity sensitive pixel. The normalized output is the transmittance of the wire grid polarizer.

The normalized transmittance as a function of the transmission axis of the linear polarizer (incident polarization angle) for the two polarization sense regions are shown in Fig. 5.

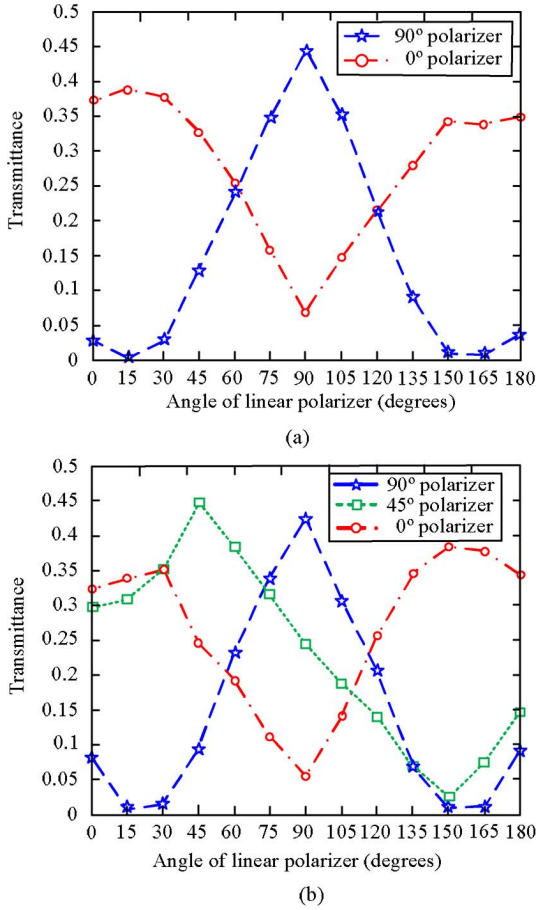

Fig. 5. 0° and 90° polarization profile. (a) Sense region 1. (b) Sense region 2.

TABLE II
Transmittance (%) and Extinction Ratio (ER)

Region	$T_{MAX}(0^{\circ})$	$T_{MIN}(0^{\circ})$	$T_{MAX}(90^{\circ})$	$T_{MIN}(90^{\circ})$	ER
1	0.389	0.07	0..444	0.01	6.3
2	0.384	0.0545	0.424	0.06	7.7

The transmitted radiance of a linearly polarized light beam varies sinusoidally as function of the polarizer transmission axis. The maximum $I_{\max}$, of the sinusoid occurs when the polarizer orientation is parallel to the orientation of the linear polarized component and the minimum $I_{\min}$ occurs when the polarizer orientation is perpendicular to the linear polarized component. The mean maximum $(T_{\max})$ and minimum $(T_{\min})$ transmittances for 0° and 90° polarization sensitive pixels in the polarization region 1 and 2 are shown in Table II.

The maximum and the minimum transmittance for the 45° sensitive pixel are 0.446 and 0.02, respectively.

V. Material Classification

A. Measurement Setup

The measurement setup for the measurements of the maximum and minimum transmitted intensities after reflection from the material surface is shown in Fig. 6

The polarized electromagnetic waves are reflected from the surface. At the boundary of the reflection surface, both the diffuse component and the specular component of the reflection of

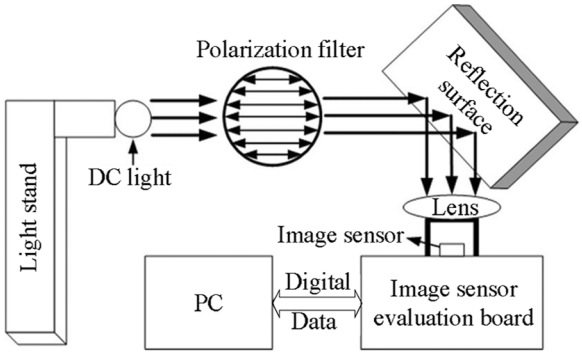

Fig. 6. Measurement setup.

the incident light are present. These reflection components are then incident on the image sensor after focusing by a lens. The analog signal from the image sensor is digitized using an external ADC and then analyzed using a PC. For the first version the analysis was done off-chip to prove the concept. The transmission axis of the linear polarization filter is varied from 0° to 90° in steps of 30° to change the polarization angle of the light reflected by the reflection surface.

At the beginning of the experiment the mean of the chosen pixel array of 20×20 without the linear polarizer is noted as in (13), which is used as a normalization factor:

$$p_{\text{avg(no linear polarizer)}}(x,y) = \frac{1}{XYN}\sum_{n=1}^{N}\sum_{x=0}^{X-1}\sum_{y=0}^{Y-1} p_n(x,y) \tag{13}$$

where X and Y are the pixel array dimensions and N is the total number of frames used to compute the mean. The normalized intensity is then obtained by dividing the mean pixel intensity with the linear polarizer (13) by the mean pixel intensity without the linear polarizer (14) shown in (15).

The mean of the acquired intensity values of the pixels sensitive to 0° and 90° in sense region 1, and of the pixels sensitive to 0°, 45°, and 90° in sense region 2, is computed for 30 frames as follows:

$$p_{\text{avg(with linear polariyer)}}(x,y) = \frac{1}{N}\sum_{n=1}^{N} p_n(x,y) \tag{14}$$

where $p(x,y)$ is the measured pixel intensity, x and y are the row and column number of the sensor array, and N is the number of frames selected:

$$\text{Normalized}p_{\text{avg}}(x,y) = \frac{\left(\frac{1}{N}\sum_{n=1}^{N} p_n(x,y)\right)}{\left(\frac{1}{XYN}\sum_{n=1}^{N}\sum_{x=0}^{X-1}\sum_{y=0}^{Y-1} p_n(x,y)\right)}. \tag{15}$$

B. Polarization Transmittance

The magnitude of oscillations of the reflected irradiance of the light after reflection is larger for dielectrics than for metals [5]. The intensity of the reflected wave is a function of the transmission axis of the linear polarizer $I(x,y:\theta)$ and oscillates between the maximum transmitted intensity $I_{\max}$ and the minimum transmitted intensity $I_{\min}$ as shown in (4). For dielectrics the Fresnel coefficients satisfy $R_p \gg R_s$ while for metals $R_p \approx R_s$. The diffuse component of reflection dominates over the specular component $I_d(x,y) \gg I_s(x,y)$ for dielectrics and thus the oscillations given by (7) and (8) vary over a larger range, while in case of metals, the oscillations are relatively smaller as the specular component of reflection dominates over the diffuse component of reflection $I_s(x,y) \gg I_d(x,y)$.

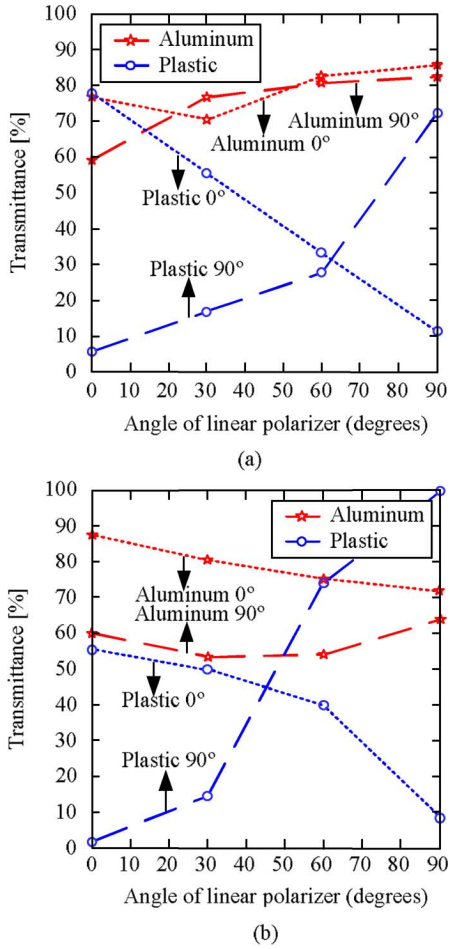

Fig. 7. Transmitted Intensity at 0° and 90° polarization sensitive pixel in sense region 1 (top) and sense region 2 (bottom).

TABLE III
TRANSMITTED RADIANCE FOR PLASTIC AND ALUMINUM

	Region 1		Region 2	
	Plastic	Alum.	Plastic	Alum.
$I_{\max}$ $I_{\min}(0)$	0.66	0.15	0.466	0.16
$I_{\max}$ $I_{\min}(90)$	0.67	0.23	0.985	0.10

Fig. 7 shows the measured transmitted irradiance in the sense regions 1 and 2 for 0° and 90° sensitive pixels for aluminum and plastic reflecting surface.

The differences between the maximum and minimum transmitted irradiances for plastic and aluminum surfaces in both regions 1 and 2 are shown in Table III.

The transmitted irradiance oscillations for plastic in sense region 1 are 190% and 340% higher than that of aluminum. In the sense region 2 they are 190% and 885% higher for 90° and 0° polarization sensitive pixels, respectively. The transmitted irradiance oscillations for plastic at both polarization sense regions

1 and 2 are much higher than those for aluminum. The differences in the transmitted irradiance are due to the difference in the reflection pattern of the light from the aluminum and plastic surfaces.

C. Material Classification Using the DOP

The light reflected from the material surface is partially polarized. Thus, the polarization state of the reflected light can be represented as a sum of a completely polarized component and a completely unpolarized component [5], [13]. When the completely polarized component is polarized perpendicular to the reflection surface, the wire grid parallel to the specular plane receives maximum light intensity while the wire grid perpendicular to the specular plane receives minimum light intensity. The minimum light intensity received by the wire grid is due to the partial transmission of the unpolarized component of the reflected light. The unpolarized component consists of the diffuse reflection and also the portion of the specular reflection which is unpolarized.

The difference between the maximum transmitted intensity and the minimum transmitted intensity given by (7) and (8) shows the amount of reflected light that is completely polarized. The minimum transmitted radiance $I_{\min}$ is one half of the magnitude of the unpolarized light reflected from the object surface. The degree of polarization is the ratio of intensity of the perfectly polarized light reflected to the total intensity of the reflected light. If $I_p(x,y)$ is the partial polarization component and $I_{\text{all}}(x,y)$ is the total reflected component then

$$\begin{aligned} &I_p(x,y) \\ &\quad = T_p^{-1}A(x,y) = T_p^{-1}[I_{\max}(x,y) - I_{\min}(x,y)] \\ &I_{\text{all}}(x,y) \\ &\quad = I_p(x,y) + T_n^{-1}B(x,y) \\ &= T_p^{-1}[I_{\max}(x,y) - I_{\min}(x,y)] + 2T_p^{-1}I_{\min}(x,y) \\ &= T_p^{-1}[I_{\max}(x,y) + I_{\min}(x,y)]. \end{aligned} \tag{16}$$

The degree of polarization is then obtained from (16):

$$\begin{aligned} \text{DOP} = \rho(x,y) &= \frac{I_p(x,y)}{I_{\text{all}}(x,y)} \\ &= \frac{I_{\max}(x,y) - I_{\min}(x,y)}{I_{\max}(x,y) + I_{\min}(x,y)} \end{aligned} \tag{17}$$

Equation (17) also indicates the portion of the reflected light which is completely polarized to the total amount of reflected light, denoting the partial polarization [5]. Equation (17) has a maximum value of 1 and a minimum value of 0. At a value of 0 the reflected light is completely unpolarized; thus, the diffuse component of the reflection dominates over the specular component. At the maximum value of 1, the reflected light is completely polarized, thus the specular component of the reflection dominates over the diffuse component.

The transmitted intensities are obtained using the measurement setup shown in Fig. 6. The degree of polarization obtained for the polarization sense region 1 and 2 is shown in Fig. 8.

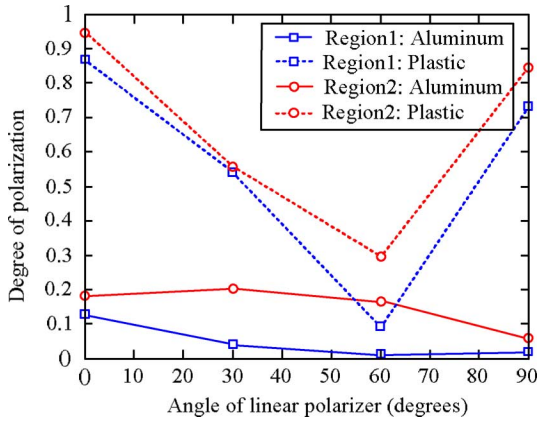

Fig. 8. Degree of polarization in sense regions 1 and 2.

TABLE IV
DEGREE OF POLARIZATION FOR PLASTIC AND ALUMINUM

	Region 1		Region 2	
	Plastic	Al	Plastic	Al
DOP (Max)	0.867	0.128	0.945	0.202
DOP (Min)	0.09	0.02	0.298	0.06

The maximum and minimum values of the DOP for the two reflecting surfaces of plastic and aluminum in the two polarization sense regions 1 and 2 are given in Table IV.

The degree of polarization is higher for plastic than for aluminum. It is observed from Fig. 8 that for plastic the maximum DOP is near 1 in both polarization sense regions, while for aluminum the maximum DOP in both polarization sense regions is less than 0.2. A higher DOP indicates higher amount of the reflected light being polarized, as stated in Section II-B that non metallic surfaces polarize the reflected light stronger than metallic surfaces.

It is further observed from Fig. 8 that as the specular angle of incidence is increased; the DOP tends to decrease for both plastic and aluminum. However, after a certain specular angle of incidence, the DOP of aluminum continues to fall but the DOP of the plastic shows a sharp rise. From (2) it is seen that R_s never vanishes but R_p becomes zero when

$$\begin{aligned} \tan(\varphi + \eta) &= \infty \\ \varphi + \eta &= \frac{\pi}{2}. \end{aligned} \tag{18}$$

From (18)

$$\begin{aligned} \sin\eta &= \sin\left(\frac{\pi}{2} - \varphi\right) \\ \tan\varphi &= n \end{aligned} \tag{19}$$

where η is the index of refraction. When the angle of incidence satisfies the condition in (19), the electric field amplitude in the reflected wave has no component which lies in the plane of incidence, meaning that the entire component R_p gets refracted. The only component in the reflected wave is the one that is perpendicular to the plane of incidence. The reflected wave is completely polarized.

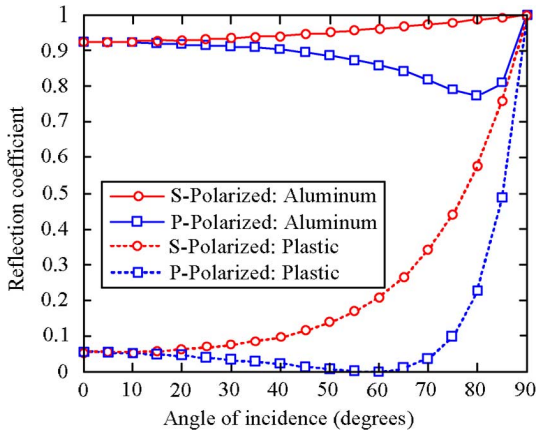

Fig. 9. Theoretical Fresnel reflection coefficients for aluminum and plastic at $\lambda = 500$ nm.

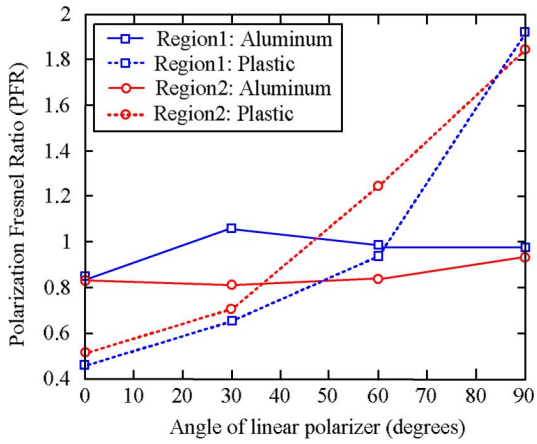

Fig. 10. Polarization Fresnel Ratio in sense region 1 and 2.

The angle of incidence φ is known as the Brewster angle. The Brewster angle for plastics is near 60°, which explains the sharp rise of the DOP of plastic around 60°. For light absorbing material like metals R_p is never 0 and thus no such sharp increase in the DOP of aluminum is observed.

D. Material Classification Using the Polarization Fresnel Ratio

The Polarization Fresnel Ratio (PFR) is the ratio of the perpendicular Fresnel coefficient to the parallel Fresnel coefficient. Wolff in [5] introduces the PFR based on Fresnel reflectance model as a metric tool to classify materials into metals and dielectrics. The Fresnel reflection and transmission coefficients in the Fresnel reflectance model are given by (2). The theoretical Fresnel reflection coefficients for aluminum and plastic are shown in Fig. 9. The Fresnel reflection coefficient for aluminum is near 1, while that for plastic varies over the entire span from 0 to 1 for different specular angles of incidence.

The Fresnel reflection coefficient R_p is 0 near the Brewster angle for plastic and thus the PFR for dielectric (plastic) can become arbitrarily large, while the PFR for metals is limited. For the electromagnetic visible spectrum from 400 to 700 nm, it has been reported that the PFR for metals usually remains below 2 for most specular angle of incidence [5].

The PFR can be derived from (7) and (8) as

$$R_s(x,y) = \frac{[I_{\max}(x,y) - T_n I_d(x,y)][R_p(x,y) + R_s(x,y)]}{T_p I_s(x,y)} \tag{20}$$

$$R_p(x,y) = \frac{[I_{\min}(x,y) - T_n I_d(x,y)][R_p(x,y) + R_s(x,y)]}{T_p I_s(x,y)}. \tag{21}$$

Dividing (20) and (21), we get

$$\frac{R_s(x,y)}{R_p(x,y)} = \frac{[I_{\max}(x,y) - T_n I_d(x,y)]}{[I_{\min}(x,y) - T_n I_d(x,y)]}. \tag{22}$$

The specular component of reflection in metals is greater than the diffuse component of reflection $I_s(x,y) \gg I_d(x,y)$ [9]. Thus, the diffuse component of reflection $I_d(x,y)$ in (22) can be neglected resulting in

$$\frac{R_s(x,y)}{R_p(x,y)} \approx \frac{I_{\max}(x,y)}{I_{\min}(x,y)}. \tag{23}$$

Equation (23) is the polarization Fresnel ratio as described in [5]. In the case of dielectrics, the Fresnel reflection coefficient R_p is very small for all specular angles of incidence, and is almost 0 near the Brewster angle. The PFR for dielectrics thus can be arbitrary large as predicted by (23). For dielectrics with specular angle of incidence very close to the Brewster angle, (23) becomes

$$\frac{R_s(x,y)}{R_p(x,y)} \gg \frac{I_{\max}(x,y)}{I_{\min}(x,y)}. \tag{24}$$

A material with significant conductivity will have a significantly reduced PFR over a large range of specular angle of incidence. Since the conductivity of metals is higher than the conductivity of dielectrics, the PFR for metals is much smaller compared to that of dielectrics. As in metals the specular component of reflection is larger than the diffuse component of the reflection, the Fresnel coefficients satisfy $R_s(x,y) \approx R_p(x,y)$ [13]. Using this condition in (5) and (6) we get $A(x,y) \ll B(x,y)$ which from (7) and (8) means $I_{\max}(x,y) \approx I_{\min}(x,y)$; thus, the PFR from (23) is nearly equal to 1 for all angles of incidence.

The $I_{\max}(x,y)$ and $I_{\min}(x,y)$ values are determined using the same measurement setup shown in Fig. 6. For varying transmission axis of the external linear polarizer, the pixel outputs averaged over 30 frames at the 0° and 90° polarization sensitive pixels are stored. The transmittance is computed by normalizing the output at 0° and 90° by the intensity at the intensity sensitive pixel in polarization sense region 1 and 2. The PFR is then calculated from the maximum and minimum transmittance. The experimentally obtained PFRs for aluminum and plastic in the polarization sense regions 1 and 2 are shown in Fig. 10.

There is a clear threshold in the PFR values for metals and dielectrics. The PFR for aluminum is in the range of 0.8 to 1 for all specular angles of incidence while the PFR for dielectrics rapidly increases near the Brewster angle. Theoretically, for a specular angle of incidence greater than the Brewster angle, the PFR for aluminum is always smaller than 2 [5]. A PFR value of

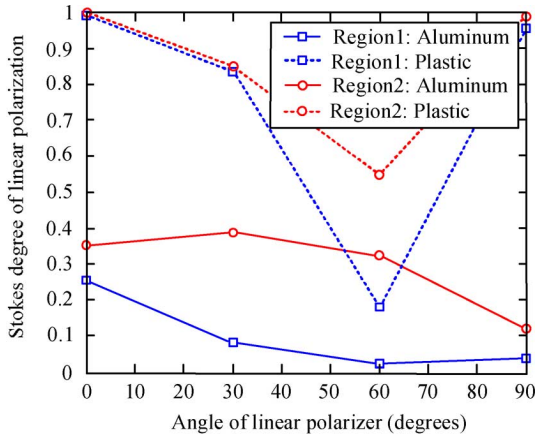

Fig. 11. Stokes parameters, degree of linear polarization in sense region 1 and 2.

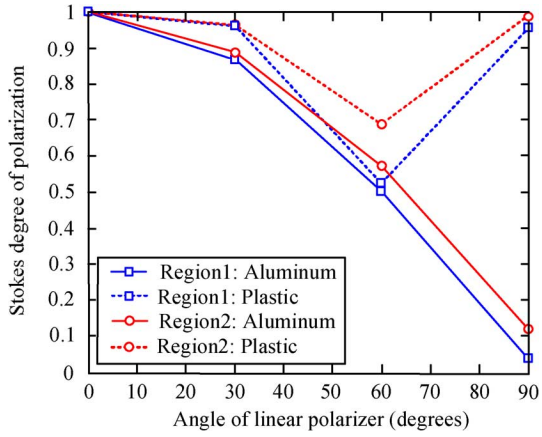

Fig. 12. Stokes degree of polarization in sense region 1 and 2.

nearly 2 can be considered to belong to a dielectric. The PFR computations using the polarization sense regions 1 and 2 offer a good match to the theoretical studies and thus can be used to classify the materials into metals and dielectrics.

E. Material Classification Using the Stokes Parameters

As stated in Section II-C, the polarization state of an electromagnetic wave can be conveniently described by a set of Stokes parameters. To the best knowledge of the authors, there is no reference available on using Stokes parameters to classify materials. Here, we use the degree of polarization and linear degree of polarization obtained from the Stokes vector to classify materials into metals and dielectrics.

The measurement setup is the same as shown in Fig. 6. The outputs of the pixels sensitive to 90° and 0° are averaged over 30 frames. Simultaneously, the output of the intensity sensitive pixels with no metal grid is also recorded for varying transmission axis of the external linear polarizer. The pixel output of the 0° and 90° polarization sensitive pixels are then normalized with the output of the intensity sensitive pixels. The normalized outputs correspond to E_{x0} and E_{y0} in (10). The degree of linear polarization is calculated using (12).

The Stokes parameters S_0 and S_1 can be obtained using (10). The degrees of linear polarization in the regions 1 and 2 are shown in Fig. 11. The Stokes degree of linear polarization for plastic has a maximum value of 1 and is higher than that for aluminum. It is further observed that the Stokes degree of linear polarization for plastics steadily decreases until it reaches the Brewster angle where the degree of polarization again increases to its maximum value. The maximum Stokes degree of linear polarization for aluminum obtained in the sense regions 1 and 2 are 0.25 and 0.38 respectively.

The degree of linear polarization for aluminum is low compared to plastic for all specular angle of incidence. Furthermore, the degree of linear polarization of plastic is found to decrease with the increase of the specular angle of incidence and a sharp rise in the degree of linear polarization is observed around the Brewster angle for plastics.

The above discussion was related to the degree of linear polarization obtained from the Stokes parameters. The Stokes degree of polarization is given by (11). The fourth Stokes parameter S_3 is usually ignored for natural light [11], since the phase information between orthogonally polarized light is difficult to calculate for natural light. Thus, (11) can be modified with $S_3 = 0$ as

$$\mathrm{DOP} = \delta = \frac{\sqrt{S_1^2 + S_2^2}}{S_0}. \tag{25}$$

S_0 and S_1 are the same as for the linear degree of polarization. S_2 is calculated from (10). $\nabla\varphi$, the phase difference in (10), is set to the specular angle of incidence.

The obtained degrees of polarization in the polarization sense regions 1 and 2 are shown in Fig. 12.

The plastic shows the similar response to Fig. 11 while the metal shows a steady decrease from the maximum value to minimum with increasing angle of linear polarizer. As the angle of specular incidence approaches the Brewster angle, the degree of polarization in case of plastics increases to its maximum value while no such behavior is observed for aluminum neither in sense region 1 nor in region 2. A threshold can be applied to the Brewster angle to classify between aluminum and plastic using the degree of polarization computed using the Stokes parameters.

F. Metal Classification Using the PFR

The Fresnel reflection theory can also be used to classify among conductive metallic surfaces. The Fresnel reflection coefficients depend on the index of refraction ε and the specular angle of incidence φ as shown in (2). The index of refraction ε is considered to be a complex number:

$$\varepsilon = n - i\kappa \tag{26}$$

where n is the simple index of refraction while κ is called coefficient of extinction. κ is a measure of how well a particular material scatters and absorbs electromagnetic waves. A material with low κ allows for easy transmission of the electromagnetic waves and vice versa. The index of refraction for dielectrics is a real number as the coefficient of extinction is negligible and thus neglected, while the index of refraction for metals is a complex number. The components of the index of refraction n and κ are related to electromagnetic physical parameters of a material surface [15] as

$$n^2 = \frac{\nu\gamma c^2}{2}\left[1 + \sqrt{1 + \left(\frac{\lambda\sigma}{2\pi c\gamma}\right)^2}\right] \tag{27}$$

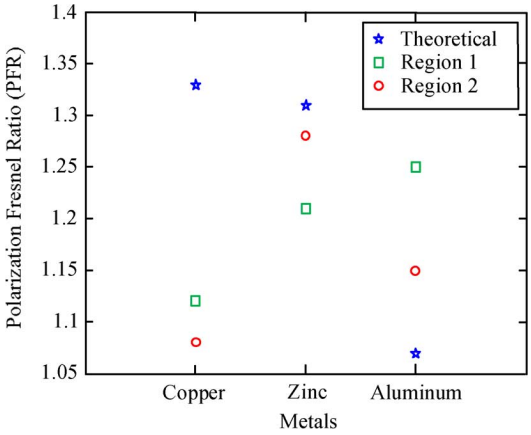

Fig. 13. Theoretical and measured PFR for copper, zinc, and aluminum in sense region 1 and 2.

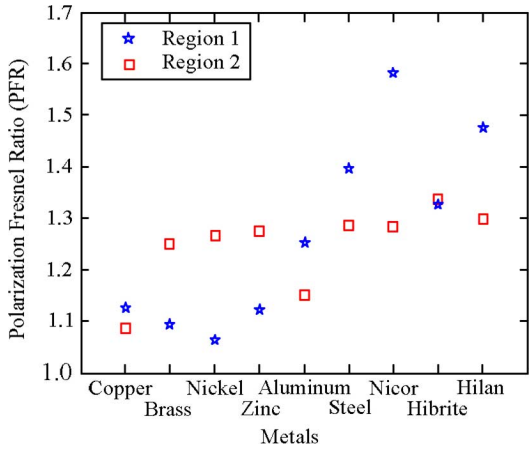

Fig. 14. Measured PFR for various metals in sense region 1 and 2.

TABLE V
THEORETICAL AND EXPERIMENTAL PFR VALUES

Metals	Max. Theoretical *PFR* [5]	Experimental *PFR*	
		Region1	Region2
Copper	1.33	1.12	1.08
Alum.	1.07	1.25	1.15
Zinc	1.31	1.21	1.28

$$\kappa^2 = \frac{\nu\gamma c^2}{2}\left[-1+\sqrt{1+\left(\frac{\lambda\sigma}{2\pi c\gamma}\right)^2}\right] \tag{28}$$

where σ is the conductivity of the material surface, υ is the electrical permittivity, γ is the magnetic permeability, λ is the incident wavelength of light, and c is the speed of light in vacuum, respectively.

From (27) and (28) it can be inferred that, with all other physical parameters remaining constant, the index of refraction increases with an increase in the conductivity of the material. Thus, it can be said that the Fresnel equations depend on the conductivity of the material surface. It was further observed in Section III-D that as the conductivity increased from dielectrics to metals, the Fresnel reflection coefficients increased thus reducing the PFR as a function of the specular angle of incidence. The variation in the conductivity among various metals will affect the Fresnel reflection coefficients which will further vary the PFR. Changes in the physical parameters in (27) and (28) for various metal surfaces would result in different reflection behavior.

The PFR for copper was found to be lower than that of zinc and aluminum in both polarization sense regions 1 and 2. The PFR discussed in Section III-D can further be extended to study the different metal surfaces of varying conductivity. The measurement set up is the same as the one shown in Fig. 6, while the reflection surface was now chosen among copper, zinc, and aluminum. The strip thickness of the metal layers used are from 0.10–1.50 mm and a width maximum of 650 mm. Table V and Fig. 13 show the theoretical and experimentally obtained PFR for copper, zinc, and aluminum in both polarization sense regions 1 and 2. The theoretical values are the maximum values where the PFR were averaged over different index of refraction corresponding to wavelengths in the visible spectrum [5].

Among the selected three metallic surfaces, the conductivity of copper (0.596×10^6/cm Ω) is the highest and aluminum (0.377×10^6/cm Ω) is more conductive than zinc (0.166×10^6/cm Ω). The higher conductivity of copper produces higher Fresnel reflection coefficients which in turns results in lower PFR, seen in the experimentally obtained PFR in both polarization sense region 1 and 2 in Fig. 13. The zinc being the less conductive should have higher PFR, as seen in polarization sense region 2. In polarization sense region 1 zinc shows lower PFR then aluminum, which could be the result of the variations in the specular angle of incidence[1] of the light source. However, we still see a clear distinction between the degrees of polarization for copper, zinc, and aluminum, and the PFR values are less than 2 as stated in [5].

To extend the study of changes in the PFR with conductivity, more metallic surfaces were selected and the experimentally obtained PFR are correspondingly shown in Fig. 14.

The lower conducting metals such as steel, hibrite, hilan, and nicor show higher PFR values in both the polarization sense regions 1 and 2, compared to highly conductive metals such as copper, zinc, and nickel. The higher PFR for low conduction materials is due to the reduced reflection and lower Fresnel reflection coefficients. A clear distinction can be observed among the PFR values of various test metal surfaces of varying conductivity.

The DOP of highly conductive materials is lower than the DOP of low conducting materials. The DOP introduced in Section III-C was also calculated for various metallic surfaces and the obtained DOP in the polarization sense regions 1 and 2 is shown in Fig. 15. The resultant plots shows similar behavior as the PFR plots.

It is observed that the DOP of metal surfaces varies between 0 and 0.25 in both the polarization sense region 1 and 2. The lower conducting metal surfaces, such as steel and its varieties occupy the higher band of the range while the lower band is occupied by highly conducting metal surfaces.

There is however a difference in behavior in the two polarizations sense regions for both the PFR and DOP measurements as seen in the Figs. 14 and 15. In region 2, the difference between the copper and other conducting materials is more pronounced

[1]The specular angle of incidence of the light source was not well controlled.

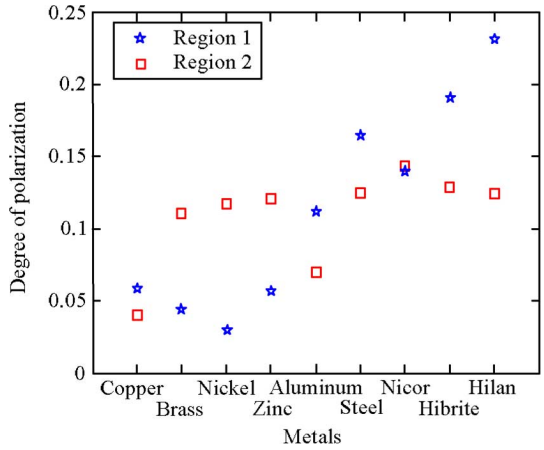

Fig. 15. Measured degree of polarization sense region 1 and 2.

than in region 1. This can be explained by considering the presence of an additional 45° linear polarizer in region 2 along with the fact that the Fresnel coefficients measured are truly a regional average. For highly reflective surfaces, the response of the 45° sensitive pixels increases the Fresnel coefficients average, thus further decreasing the PFR and DOP. For copper $R_s(x,y) \approx R_p(x,y)$ while for other conducting materials the average $R_s(x,y)$ increases due to the 45° polarizer response compared to $R_p(x,y)$, thus increases the PFR and DOP. For very low conducting surfaces the 45° sensitive pixels does not effect the Fresnel coefficient measurements thus measured average $R_s(x,y)$ decreases reducing the PFR and DOP.

VI. Conclusion

We have designed a CMOS image sensor using a wire grid to analyze polarization information. The various orientation angle of the grid measured the different polarized light intensities. An extinction ratio of 6.3 and 7.7 was achieved in the two sense regions of the sensor.

The sensor was shown to be able to differentiate among various reflecting surfaces based on the intensity variations due to the polarization pattern of the reflected light. The polarization state for the diffuse and specular components of the reflection depend on the reflecting surface, and the measurement of polarization state of the reflected light serves as an indicator for the type of material surface. The magnitude of oscillations of the maximum and minimum transmitted irradiance due to the variation in the reflection pattern of metal and dielectric surface was found to be useful in classifying among them. Various other measurement metrics, such as the degree of polarization and the polarization Fresnel ratio, were shown to measure the variations in the reflection pattern of the metal and dielectric surface. The degree of linear polarization obtained using Stokes parameters is also shown to be able to classify surfaces into metal and dielectrics.

The polarization of the reflected component of the light wave varies with the conductivity of the metallic surface and this was further explored and shown to be able to serve as a tool to classify among highly conductive and lowly conductive metallic surfaces.

The transmitted intensities of the reflected light were measured for a single angle of incidence of the light ray. The measurement of the PFR at each pixel is not very accurate when the diffuse component of the reflection dominates over the specular component, in such scenario the measurement of the reflected transmitted intensities for varying angle of incidence of the light ray would serve to increase the resolution and the sensitivity of the PFR measurement.

Acknowledgment

The authors would like to thank DALSA for providing the test table to characterize the sensor, INVOMEC for helping with the fabrication of the chip, A. Mierop of DALSA, G. Meynants of CMOSIS, and P. Merken for their valuable contributions to the project.

References

[1] G. Klinker, S. Shafer, and T. Kanade, "Using a color reflection model to separate highlights from object color," in *Proc. IEEE 1st Int. Conf. Comput. Vis.*, 1987, pp. 145–150.
[2] S. Shafer, "Using color to separate reflection components," *Color Res. Applicat.*, vol. 10, pp. 210–218, 1985.
[3] G. Healey and W. E. Blanz, "Identifying metal surfaces in color images," in *Proc. SPIE Conf. Opt., Electro-Opt., Sens.*, 1988.
[4] G. Healey and T. O. Binford, "Predicting material classes," in *Proc. DARPA Image Understanding Workshop*, 1988, pp. 1140–1146.
[5] L. B. Wolff, "Polarization based material classification from specular reflection," *IEEE Trans. Pattern Anal. Mach. Intell.*, vol. 12, no. 11, pp. 1059–1071, Nov. 1990.
[6] H. Chen and L. Wolff, "Polarization phase based method for material classification and object recognition in computer vision," *Int. J. Comput. Vis.*, vol. 28, no. 1, pp. 45–56, 1999.
[7] E. Hchet and A. Zajak, *Optics*, 3rd ed. London, U.K.: Longman, Addison-Wesley, 1988.
[8] D. D. Malacara, *Physical Optics and Light Measurements*. San Diego, CA: Academic, 1989, p. 157.
[9] T. Tokuda, H. Yamada, H. Shimohata, K. Sasagawa, and J. Ohta, "Polarization-analyzing CMOS image sensor with embedded wire grid polarizer," in *Proc. Int. Image Sens. Workshop*, 2009.
[10] T. Tokuda, H. Yamada, K. Sasagawa, and J. Ohta, "Polarization-analyzing CMOS image sensor using monolithically embedded polarizer for microchemistry system," in *Proc. IEEE Int. Symp. Circuits Syst.*, 2009, pp. 313–316.
[11] V. Gruev, J. van der Spiegel, and N. Engheta, "Advances in integrated polarization imaging sensors," in *Proc. IEEE/NIH LiSSA Workshop*, 2009, pp. 62–65.
[12] G. S. Smith, *An Introduction to Classical Electromagnetic Radiation*. Cambridge, U.K.: Cambridge Univ. Press, 1997.
[13] S. Tominaga and A. Kimachi, "Polarization imaging for material classification," *Opt. Eng.*, vol. 47, no. 12, pp. 123–201, 2008.
[14] J. N. Damask, *Polarization Optics in Telecommunications*. New York: Springer, 2005, p. 22.
[15] R. Siegal and J. R. Howell, *Thermal Radiation Heat Transfer*. New York: McGraw-Hill, 1981.

Mukul Sarkar (S'10) received the B.E. degree from Andhra University, Andhra Pradesh, India, in 2002, and the M.Sc. degree from the University of Technology, Aachen, Germany, in 2006. He is currently working towards the Ph.D. degree in the Electronics Instrumentation Laboratory, Faculty of EEMCS, Delft University of Technology, Delft, The Netherlands, with Prof. A. J. P. Theuwissen on the subject of biologically inspired CMOS image sensors.

Between 2003 and 2005, he worked in the Philips Institute of Medical Information, Aachen, Germany, as a Research Assistant in detection and analysis of bio-signals. His current research interests includes biological-inspired vision systems for motion detection and navigation.

David San Segundo Bello (M'98) received the M.Sc. degree from the Universitat Autònoma de Barcelona, Barcelona, Spain, and the Ph.D. degree from the University of Twente, Enschede, The Netherlands. His Ph.D. topic was the design of pixel-level ADCs for hybrid X-ray detectors. He did this work in collaboration with the Dutch Institute of High Energy Physics (NIKHEF) and CERN.

Between 2004 and 2008, he was a Design Engineer in the Wireline Group of Infineon Technologies (currently Lantiq), where he was involved in the design of line drivers and ADCs for xDSL applications. Since 2008, he has been with imec, Leuven, Belgium, in the design of electronic systems and ICs for image sensors. His current research interests are image sensor systems, high-resolution data converters, and CMOS sensor readout electronics.

Chris van Hoof (M'91) received the Ph.D. degree in electrical engineering from the University of Leuven, Leuven, Belgium, in 1992 in collaboration with imec.

He is Director of the HUMAN++ program and Director of Integrated Systems at imec, Leuven, Belgium, and at the Holst Center, Eindhoven, The Netherlands. After the Ph.D. degree, he became successively head of the Detector Systems Group (in 1998), Director of the Microsystems and Integrated Systems Department (in 2002), Program Director of Smart Implants (in 2007) and HUMAN++ (in 2009). His research concerns design, technology and applications of body-area networks and heterogeneous integration for medical and imaging applications. Since 2000, he also has been a Professor at the University of Leuven. He has authored and coauthored over 250 publications.

Albert J. P. Theuwissen (M'82–SM'95–F'02) was born in Maaseik, Belgium, on December 20, 1954. He received the M.S. and Ph.D. degree in electrical engineering from the Catholic University of Leuven, Leuven, Belgium, in 1977 and 1983, respectively.

From 1977 to 1983, his work at the ESAT-Laboratory of the Catholic University of Leuven focused on linear CCD image sensors. In 1983, he joined the Micro-Circuits Division, Philips Research Laboratories, Eindhoven, The Netherlands, and was involved in research in the field of solid-state imaging, which resulted in the project leadership of respectively SDTV- and HDTV-imagers. In 1991, he became Department Head of the division, Imaging Devices. In March 2001, he was appointed as part-time Professor at the Delft University of Technology, Delft, The Netherlands, where he teaches courses in solid-state imaging and coaches Ph.D. students on CMOS image sensors. In 2002, he joined DALSA Corp. as the company's Chief Technology Officer and continued to be its Chief Scientist after retirement from DALSA. In 2007, he started his own company, Harvest Imaging, which focuses on consulting, training, teaching, and coaching in the field of solid-state imaging technology. In 2006, he cofounded ImageSensors, Inc. (a non-profit entity) to address the needs of the image sensor community. He is author or coauthor of over 120 technical papers and issued several patents. He authored a textbook *Solid-State Imaging with Charge-Coupled Devices* (Springer, 1995).

Prof. Theuwissen was a member of the International Electron Devices Meeting paper selection committee in 1988, 1989, 1995, and 1996. He is co-editor of the IEEE TRANSACTIONS ON ELECTRON DEVICES special issues on Solid-State Image Sensors, May 1991, October 1997, January 2003 and November 2009, and of IEEE Micro special issue on Digital Imaging, November/December 1998. In 1998 and 2007 he became an IEEE ED and SSCS distinguished lecturer. He acted as general chairman of the IEEE International Workshop on Charge-Coupled Devices and Advanced Image Sensors in 1997, 2003, and 2009. He is member of the Steering Committee of the aforementioned workshop and founder of the Walter Kosonocky Award, which highlights the best paper in the field of solid-state image sensors. He was a member of the technical committee of the European Solid-State Device Research Conference and of the European Solid-State Circuits Conference. Since 1999, he has been a member of the technical committee of the International Solid-State Circuits Conference for which he acted as secretary, vice-chair, and chair in the European ISSCC Committee and also a member of the overall ISSCC Executive Committee. Recently, he has been elected to be International Technical Program Chair vice-chair and chair for, respectively, the ISSCC 2009 and ISSCC 2010. In 2008, he received the SMPTE's Fuji Gold medal for his contributions to the research, in the field of solid-state imaging. He is member of editorial board of *Photonics Spectra* and is a member of SPIE.